HYBRID AUTOMATA APPROACH IN MODELING THE ROLE OF PATHWAYS BETWEEN SINOATRIAL NODE (THE HEART PACEMAKER) AND ATRIUM*

Danuta Makowiec

Institute of Theoretical Physics and Astrophysics, University of Gdańsk
Wita Stwosza 57, 80-308 Gdańsk, Poland

Zbigniew R. Struzik

Graduate School of Education, The University of Tokyo, Japan
and
RIKEN Advanced Center for Computing and Communication, Japan

(Received January 2, 2019)

The functional anatomy between the human right atrium and the sinoatrial node (SAN) still remains an open problem under investigation. There are contradictory hypotheses of how the SAN is electrically connected to the atria. We use an accurate and efficient approach of the so-called hybrid automata to investigate electrophysiological aspects of the atria–SAN coupling. This approach allows us to simulate the tissue heterogeneity preserving high accuracy of cellular dynamics as a continuous time Markov process with transitions representing short-lived transient behaviors. Our simulations suggest that there is an optimal organization of the SAN exit pathways to the atrium, which here we have identified to be smaller than 1/4 (with maximum at 1/16) of all possible SAN exits to the atrium. At this fraction, the system provides almost always normal heart rhythm, if only the density of connections between cells is high enough and the cells perform the excitation with high probability. Deviations from these conditions could result in tachycardia or in a loss of rhythm.

DOI:10.5506/APhysPolBSupp.12.111

1. Introduction

The human heart is a complex system and its study involves multiple physical and chemical aspects. The electrical activity is generated in the sinoatrial node (SAN) — a complex of specialized cells located in the

* Presented at the Summer Solstice 2018 Conference on Discrete Models of Complex Systems, Gdańsk, Poland, June 25–27, 2018.

upper part of the right atrium. Then it spreads over the atria stimulating an atrial contraction which finalizes with excitation of the atrioventricular node (AVN). The AVN is another complex of specialized cells located in the bottom part of the right atrium. The AVN is the gate by which the wave of excitation extends to ventricles for the massive mechanical contraction of main parts of the heart muscle. Any disturbance in the impulse propagation through the cardiac muscle is called arrhythmia.

The human right atrium anatomy is still under investigations. The conducting system of atria is specific due to the cell-to-cell connections, and special cell arrangement [1]. This altogether permits rapid transmission of impulses. However, there are contradictory hypotheses of how the SAN is electrically connected to the atria. The first one states that the SAN is electrically insulated from the surrounding atria by a structural border of fibrosis, fat layers, and myocyte discontinuity, and the functional and structural connection between the SAN and atria is limited to discrete SAN exit pathways [2–4]. The second hypothesis proposes that the SAN and atrial cells are extensively connected by diffuse digitations of the SAN border with the atrial myocardium, and no discrete pathways exist [5]. Both hypotheses are supported by optical mapping experiments.

The problem of the SAN–atrium connection can be seen as a distinctive example of the complex interplay between a network of intercellular couplings and the organ functionality. To test this hypothesis, computer simulations have been performed by Kharche *et al.* [6]. They have found that the insulating border with limited number of SAN–atrium path exits promotes SAN–atria tachycardia, *i.e.*, the arrhythmia resulting with the fast rhythm.

The models which use the discrete approach are sometimes considered as inadequate due to their simplicity when compared to the biophysically detailed models [7, 8]. However, this is not accurate since for a given set of differential equations, there exists a technique — hybrid automata, allowing to construct an abstract model which preserves all the properties of interest. Intuitively, the short-lived, transient behaviors are represented as discrete transitions. Thanks to this approximation, the computational efficiency of the hybrid automata is high and, therefore, one is able to test variate predictions about heart electrophysiological behavior with relatively low computational cost. The physiological motivation of the hybrid automata approach is discussed in [9]. This paper is devoted to further promoting and disseminating this approach. Subsequently, we present the numerical motivation together with the details of our implementation aimed at testing the impact of the limits in pathways between the sinoatrial node and the right atrium on the rhythm of heart contractions. The implementation of the program: executable files and the C++ code are provided via the GitHub license [10].

The main result of our simulations is that there exists the optimal organization of the SAN exits. In particular, we have found that the fraction of all possible exits should be smaller than 1/4. In these conditions, the resulting rhythm is almost always normal if the dynamics is only slightly perturbed by cellular refuse to excitations and when the density of intercellular connections is sufficiently high. Deviations from these conditions could result in the transition to tachycardia — a very fast heart rhythm, or in the loss of rhythm. Similar results have been discussed in [11], however they have been obtained for the SAN of different (smaller) shape.

2. On modeling the cardiac tissue

2.1. Biological background

For non-pacemaking excitable cells of atria or ventricles, action potentials (APs) are externally triggered events [12]: a cell fires the AP as an all-or-nothing response to a supra-threshold stimulus, see Fig. 1. Each AP follows the same sequence of phases and maintains approximately the same magnitude regardless of the applied stimulus. After an initial step-like increase in the membrane potential, the AP lasts for hundreds of milliseconds. Evidently, the AP of a typical ventricular cardiac cell is distinct from a typical atrial cardiomyocyte. In particular, the human atrial action potential typically exhibits a triangular shape, while the ventricle cells show a spike-and-dome shape with a prominent plateau phase. Moreover, this shape changes from cell to cell. The atrial action potential duration at 90% repolarization (APD_{90}) shows variations of between 150 and 500 msec [13]. The

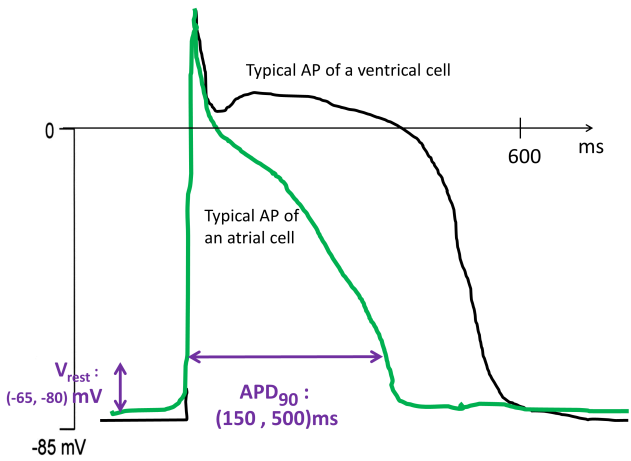

Fig. 1. (Color online) The AP for a typical myocyte of the atrium (gray/green) and ventricle (black). The uncertainty in the shape of the atrial cell AP, expressed by a variety of action potential duration APD_{90}, is displayed. (Drawn after [13].)

atrial resting membrane potential (V_{rest}) has been found to vary between -65 and -80 mV, and is more depolarized than in the human ventricle. Maximum upstroke velocities (V_{max}) for atrial action potentials have been experimentally reported to vary between ≈ 150 and 300 V/s in contrast to higher values of 300 to 400 V/s for human ventricular cells.

2.2. Continuous modeling and its limitations

Mathematical and computational models of cardiac physiology have accompanied the cardiac electrophysiology for many years. The Luo–Rudy model [14, 15] is the cardiac cell model which reconstructs the real AP from physiological transduction processes going on in the cellular membrane. The base comes from the Hodgkin–Huxley description of the ion-channel dynamics. However, the model is enriched by a much larger number of ion currents and by considering other elements of cellular electrophysiology such as active ions pumps, intercellular compartments for calcium transport, and calcium buffers. From http://www.physiome.org/jsim/models/webmodel/NSR/Luo-Rudy/ or paper of Miller *et al.* [16] one can learn about a variety of models derived from the original Luo–Rudy idea.

While these models more and more accurately reconstruct a given cell electrophysiology, they hardly manage the problem of the large variability in cellular activity [17] and the problem of the anatomical and electrophysiological heterogeneous structure of the atria, especially the right atrium [18, 19] on which the atrial function strongly depends [20]. At least, the specificity of the two clusters built of self-exciting myocytes: the SAN and the AVN has to be taken into account. Then, the conduction bundles on the right atrium: *crista terminalis* (CT) which go along the SAN and lead to the AVN, should be considered because myocytes of CT are aligned longitudinally what evidences their preferential conduction. Finally, the large part of the right atrium is formed in a comb-like fashion by the pectinate muscle (PM). In contrast, it is not possible to infer the myocyte orientation in PM. Altogether this complex anatomy makes difficult or even impossible setting the so-called typical properties and/or typical conditions.

2.3. Grid models

In the series of papers of the team of Manchester University [7, 21], the mixed approach has been used. The propagation of the AP is considered on the numerical grid made of automata. Eighteen distinct automata have been applied to capture the diversity of the right atrium tissue.

In [22], Podziemski and Żebrowski considered an even simpler model of the atria architecture. Namely, a two-dimensional square plane has been used to represent the atrial geometry. Such modeling allowed them to ar-

range directly important anatomical details necessary to study the development of arrhythmias. In particular, the matrix consisting of 100×100 simulation cells — representing 8 cm $\times$ 8 cm, what can be compared to the human right atrium size, was divided into dedicated regions: the SAN, AVN and regions of normal atrial conductive tissue in between. The two sets of equations were used: FitzHugh–Nagumo [23, 24] and Fenton–Karma [25] to simulate the ion-channels activity of cardiac cells and intercellular interactions. These two dynamics are the phenomenological simplification derived from the cellular models. They are concentrated on capturing the AP shape and, therefore, involve significantly fewer equations and fewer parameters than, *e.g.*, Luo–Rudy approach.

The cellular grid approach has been also used by Kharche *et al.* [6] to simulate the effect of limitations in SAN–atrium exits pathways. In particular, a plane of 128×128 cells evolving according to the Fenton–Karma differential equation has been considered. The SAN cells were represented as the island on the see of atrial cells, isolated from the atria or with few (four) exits.

2.4. Cellular automata approach

In the classical cellular automata model of excitation considered by Greenberg and Hastings in 1978 [26], each automaton, placed on some regular lattice, has three states: active A, firing F and refractory R, see Fig. 2. An automaton in the active state becomes firing if a number of neighbors in the firing state exceeds a certain threshold. Then, an automaton moves from firing to the refractory state, and after completing the refractory state, it returns to its original state of being active. It is known that a homogeneous network of such automata is characterized by the threshold mechanism which produces a large amplitude response to a sufficiently strong stimulus [26].

Fig. 2. An excited automaton in the active state becomes firing. Then it moves to the refractory state and spends there APD steps, after which it returns to its original state of being active.

Recently, a square lattice cellular automata model has been proposed by Christensen *et al.* [27, 28] which reproduces the known characteristics of the atrial fibrillation. In particular, the model considers vertically con-

nected automata, while horizontal connections are left rare and random. All automata are identical except the automata from the borderline, where the self-excited automata are placed to mimic the SAN. Moreover, some of the automata, chosen at random, have been assumed as dysfunctional — these automata with some probability could refuse the excitation. Simulations have provided that dysfunctional cells together with the decrease of the density of horizontal connections might block the propagation of the wavefront, what then could induce the backward wavefront which, at certain topological circumstances, starts up the reentrant circuit.

2.5. Hybrid automaton (HA)

It occurs that one can benefit from the development of abstraction techniques which, for a given system of non-linear differential equations, allows to construct a model which preserves all the properties of interest. This promising technique is hybrid automata [29]. The continuous in time evolution is broken into few phases: states, with a rather smooth dynamics. The short-lived, transient behaviors are replaces with discrete transitions between states.

Formally, for a finite set of environment events Σ affecting an automaton or sent by an automaton, a hybrid automaton is defined as a tuple [30]:

$$\mathcal{A} = \{G, X, init(), inv(), flow(), jump(), event()\}$$

consisting of:

(i) $G = (V, E)$: a directed graph with a set of vertices V, called states, and a set of edges E, called transitions;

(ii) $X = \{x_1, \ldots, x_n\}$: a set of real-valued variables;
$\dot{X} = \{\dot{x}_1, \ldots, \dot{x}_n\}$: a set of the first order derivatives of X with respect to the time with time being a continuous global variable;
$X' = \{x'_1, \ldots, x'_n, \dot{x}'_1, \ldots, \dot{x}'_n\}$: a set with values of X and $\dot{X}$ attained after the transitions, *i.e.*, initial values for the evolution in the next state;

(iii) functions labeling graph vertices:

$$init : V \to P(X),$$
$$inv : V \to P(X),$$
$$flow : V \to P(X \cup \dot{X}),$$

and functions labeling graph edges:

$$event : E \to \Sigma,$$
$$jump : E \to (Guard, Action) = (P(X \cup \Sigma), P(X')),$$

where $P()$ denotes any predicate logic about the variable.

Intuitively, an automaton spends the time in its state v from V, where it updates its variables $x, \dot{x}$ according to the flow predicate $flow(v)$. The jumps $jump(e)$ *i.e.* transitions $e = (v, w)$ are instantaneous, where v is the beginning state and w is the end state of the transition. A jump along e is taken whenever the jump's guard $jump(e).guard$ is enabled for the current values of variables X, or the invariant of the current state $inv(v)$ is unsatisfied.

The HA has a natural graphical representation as a state transition diagram, with control modes as the states and control switches as the transitions. Flows and invariants (usually predicates are written within curly braces) appear within the states (as state labels), while jump conditions (described in square brackets) and actions appear around the edges (as transition labels).

2.6. Luo–Rudy model by HA

The so-called empirical method can be used to reconstruct the Luo–Rudy model with as few continuous variables as possible, but still accurately representing cell-excitation features [30, 31]. This method follows the curve-fitting technique, where the curve being fitted can be restored by a set of linear ordinary differential equations of the form of $\dot{v} = Cv$ with $v = (v_1, v_2, v_3)$. The variables $v = (v_1, v_2, v_3)$ are not directly related to the variables of the differential equations of the Luo–Rudy model, but they represent the degrees of freedom.

In the case of an atrial myocyte with the AP of the triangular shape, the HA can be proposed as follows, see Fig. 3:

Σ: the set of environment events consists of one real variable $\{V_S\}$, which describes the strength V_S of the external stimulation;

G: the graph is built of three vertices, $V = \{s_0, s_1, s_2\}$, which are called active, firing and refractory, respectively, and of four transitions between states, $E = \{s_0 \to s_1, s_1 \to s_2, s_2 \to s_0, s_0 \to s_0\}$;

X: the set of four real variables $\{v_1, v_2, v_3, v\}$, their derivatives $\{\dot{v}_1, \dot{v}_2, \dot{v}_3, \dot{v}\}$, and reset values $\{v_1', v_2', v_3', v'\}$.

labels: $init()$, $inv()$, $flow()$, $event()$, $jump()$ to vertices and edges are given in Fig. 3.

A system of linear differential equations is defined on v_1, v_2, and v_3 variables in each state. The membrane voltage $v = v_1 - v_2 + v_3$ is used to control transitions. The value of V_S describes a stimulation event from the environment. The state invariants are given below the differential equations

describing the membrane voltage. The transitions described by the jump conditions depend on the three model-specific constants: threshold voltage for the excitation V_{T}, overshoot voltage V_{O} in response to the excitation, and repolarization voltage V_{R} which sets the resting membrane potential.

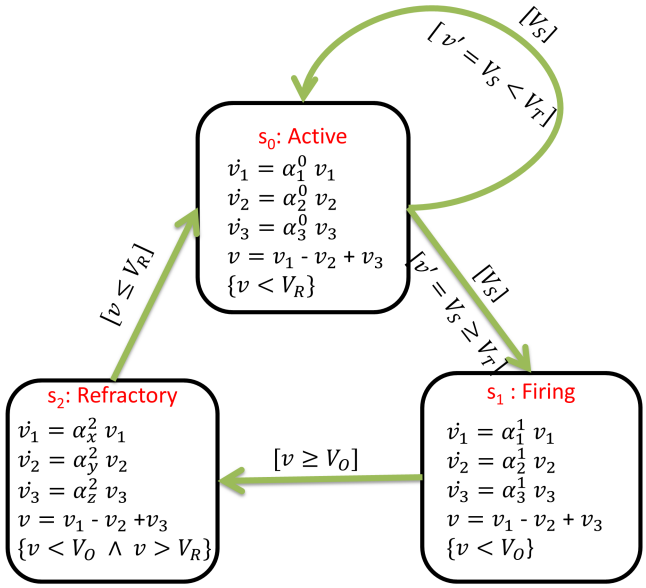

Fig. 3. The graph of HA which provides the AP resulting from the Luo–Rudy dynamics.

In Fig. 4, we plot the time dependence of v variable obtained from the HA evolution described in Fig. 3. Stimulations V_{S} were injected at random in time and value. The values of coefficients were chosen to best reveal the

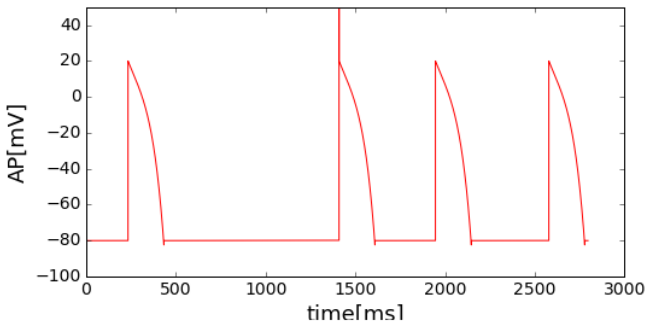

Fig. 4. The AP obtained by solving the systems of ordinary differential equations defined by $flow()$ functions in HA approach. The excitations were at random.

known properties the AP of an atrium myocyte, *i.e.*, $a_1^0 = a_2^0 = a_3^0 = 0.001$, $a_1^1 = 200, a_2^1 = 0, a_3^1 = 100$, $a_1^2 = -0.01, a_2^2 = 0.013, a_3^2 = 0.008$, $V_S = 20$, $V_R = -80, V_O = 20$. The above model at the given values of parameters very accurately reproduces the membrane potential of a myocyte. Moreover, the square lattice of such automata provides results very efficiently, see [31], namely ten times faster than with the full Luo–Rudy equations.

3. Timed automata model of atrial tissue

3.1. Myocyte AP by timed automata

It is easy to see that in the case of the HA revealing the Luo–Rudy model, the real variables v_1, v_2 and v_3 behave regularly in each state, *i.e.*, they depend on time in a linear way approximately. For this reason, one can say that state properties depend only on the time spent in this state. Therefore, instead of solving computationally demanding differential equations, one needs to regard the passage of time. This simplification leads to the notion of timed automata (TA) [32, 33].

Formally, for a finite set of environment events Σ, a timed automaton is defined as a tuple [30]:

$$\mathcal{A} = \{G, X = \mathcal{C}, init(), inv(), jump(), event()\}$$

where

(i) $G = (V, E)$ is a directed graph with a set of vertices V, called states, and a set of edges E, called transitions;

(ii) $X = \mathcal{C} = \{x_1, \dots x_n\}$ is a set of real-valued variables, called clocks, which in each time step advance the values by 1 or reset them to 0;

(iii) the function $init()$ is a subset of Σ, and remaining functions over states and transitions: $inv : V \to ClockConstriants$, $event : V, E \to \Sigma$, $jump.Guard : E \to ClockConstriants$ and $jump.Action : E \to Clock.Reset$ are labeling the graph vertices and edges by predicates driven by clocks.

Accordingly, the timed automaton, which represents the myocyte dynamics, is defined on the three state space with four edges, similarly to the HA presented in Fig. 3. However, instead of the three real variables v_1, v_2, v_3 and the set of differential equations driving their evolution, the timed automaton needs one clock variable t, see Fig. 5. The external stimulation is quantified by N_S. The jump conditions are defined by the three clock constraints: (1) a threshold N_F for the response to the external stimulation, (2) time steps spent in state s_1 *i.e.* firing f, (3) time steps spent in state

s_2 *i.e.* refractory r. The fourth constant a is introduced to limit time steps spent in the active state s_0. Notice that with a constant, we have a possibility to mimic the self-excitation of a cell what is important in the case the automaton simulates the SAN myocyte.

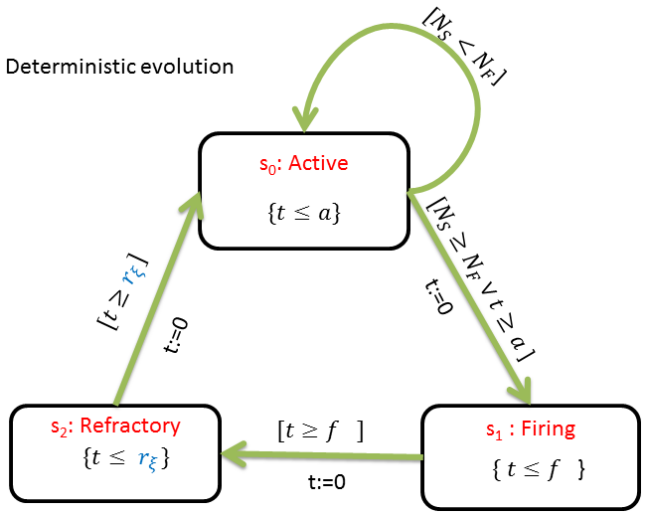

Fig. 5. A timed automaton which restores the AP properties resulting from the Luo–Rudy dynamics for an atrial cell.

Moreover, to include to the model the cell-to-cell variability, we consider $r = jump.Guard(s_2 \to s_0)$ the length of APD as a random variable. We assume that $r = r_0 + \xi$, where r_0 is fixed but ξ is a random variable with the uniform distribution $U[0, R]$. So, in the initial step, each automaton obtains its ADP value $r_0 \le r \le r_0 + R$ with which it performs the evolution. This value is assigned to a cell independently of other cells.

The ability of self-excitation of the SAN-cells is simulated by setting the parameter $a = jump.Guard(s_0 \to s_1)$ finite. Consequently, the SAN cell intrinsic dynamics is periodic with the period $T_{\mathrm{SAN}} = f + r + a$. In the case of atrial cells, the value of $jump.Guard(s_0 \to s_1) = \infty$ in all simulations. These cells settle at the s_0 state after the excitation driven by the external event.

The initial state of each automaton is set at random. In Fig. 6, we present the procedure with which the automata of the system are initialized.

Finally, the stochastic evolution is introduced in order to simulate the impairment of a cell. Namely, at any time step, a cell can refuse the excitation with probability p_{refuse}, see the label for the transition $s_0 \to s_1$ in Fig. 7. Consequently, the transition $s_0 \to s_1$ is performed if two conditions

are satisfied: a randomly chosen number $\xi \in U(0,1)$ is greater or equal to p_{refuse} and the external excitation N_S is stronger than the threshold value N_F. Otherwise, a cell stays in state s_0.

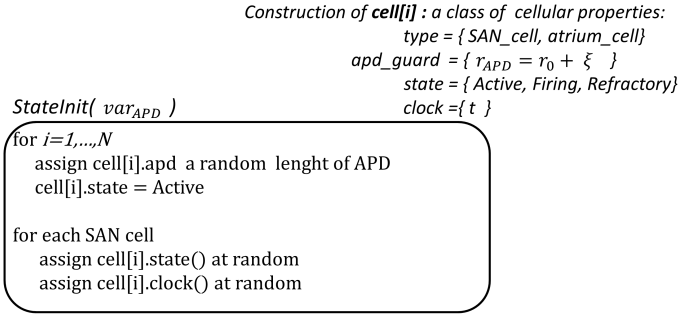

Fig. 6. The *StateInit()* procedure and variables involved which set initial states to cells.

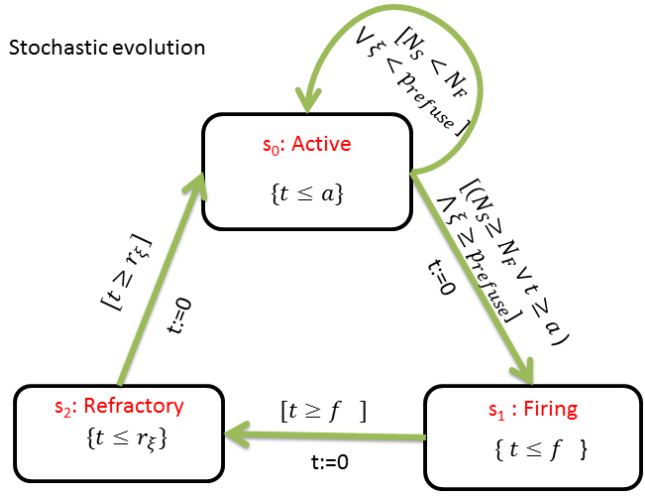

Fig. 7. A stochastic timed automaton where the extra condition for cellular excitation is introduced — the excitation is performed with probability p_{refuse}.

3.2. Right atrium architecture by stochastic square lattice network

Two types of TA cells: the SAN cells and the atrial cells, are organized in a square lattice of $L \times L$ size in a way shown in Fig. 8.

Each cell interacts with the same nearest neighbors selected in the initial step. These neighbors are chosen at random from the Moore neighborhood with probabilities p_{V}, p_{H} and p_{L} for vertical, horizontal and lateral connec-

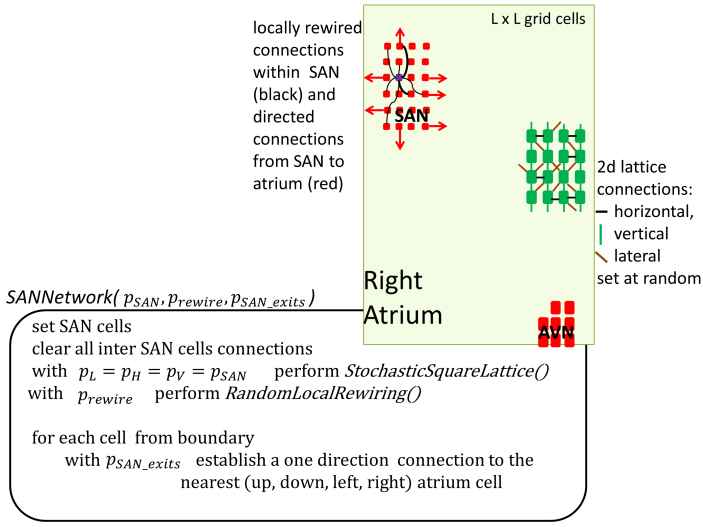

Fig. 8. A general architecture of the right atrium model and the main procedure applied in the construction of inter-cellular links in the SAN, and between the SAN and atrium. The atrial cells are regularly arranged in vertices of 2D square lattice. They are stochastically interconnected within the Moore neighborhood. The SAN cells are also randomly interconnected. Additionally, the local rewiring algorithm, see Fig. 9, is applied to each cell to mimic a free architecture of connections between the SAN cells.

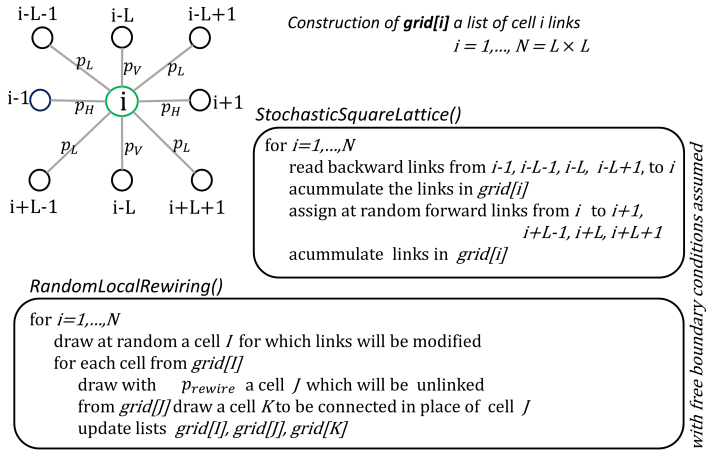

Fig. 9. Construction of intercellular links: algorithm for stochastic lattice connections and algorithm of local rewiring, for details, see [34].

tions, respectively. However, respecting the known physiology of the atrium (the crista terminalis arrangement), we assume that all atrial cells are connected vertically, *i.e.*, $p_{\mathrm{V}} = 1$. The densities of horizontal p_{H} and lateral p_{L} connections are the model parameters.

Additionally, since the main concern of our modeling is the SAN–atrium connection, then for each cell from the SAN boundary with probability $p_{\mathrm{SAN\_exits}}$ a directed connection to the nearest atrial cell is established.

In the case of the SAN cells, there is not any direction in favor. In order to imitate more casual architecture of the SAN, the algorithm of *RandomLocalRewiring()* is performed [34]. It results in locally modified neighborhoods. In particular, a given link can be rewired to the next neighbor, see Fig. 9 for details.

3.3. Model summary

Let us consider a network of timed automata $A_{i,k}$ where $i = 1, \ldots, N$ means its vertex in the network and $k \geq 0$ counts the time steps in the system. Each $A_{i,k}$ is a continuous time Markov process on the state space $V = \{s_0, s_1, s_2\}$, where the graph in Fig. 7 is the transition graph of the embedded chain. In particular, the continuous intrinsic evolution of each automaton is defined by the $flow()$ predicates, which here mean advancing the clock variable t at the constant rate in all automata.

Let $A_{i,k} = (v, t)$, where $v \in V$, $t \in \mathcal{C}$. Let $E_v = \{e \in E : e = (v, w_e)\}$ be a set of edges coming out of the state v. The jump along the $e \in E_v$ to the state w_e is performed if either $inv(v, t) == False$ or $jump.guard(e, t) == True$. Notice that the guards of edges are chosen in a way that ensures deterministic performance of the automaton cycle — there is only one outgoing edge. The stimulation threshold N_F for the transition $s_0 \to s_1$ means the count of nearest neighboring cells in state s_1. We call the automaton stochastic when with some probability $p_{\mathrm{refuse}} > 0$, the transition $s_0 \to s_1$ is not performed.

Our model is stochastic because of (1) stochastic setting of r_ξ values (our automata have different APD) and (2) stochastic arrangement of inter automata connections. The stochasticity in connections leads to the local inhomogeneity by procedure of rewiring. Additionally, the architecture of the system is globally heterogeneous due to the presence of the SAN and AVN with the fixed shape, consisting of automata with distinct from the atrium automata arrangement of connections and distinct (cyclic) intrinsic evolution. Also the limits in one-way paths for the impulse exits from the SAN effects in global system heterogeneity. All this randomness results from the initial conditions and the choice of model parameters, *i.e.*, r_ξ, p_{V}, p_{H}, p_{L}, size and location of the SAN, p_{rewire}, and $p_{\mathrm{SAN\_exits}}$. Moreover, the evolution of each automaton is stochastic because of the random execution with p_{refuse} of the transition $s_0 \to s_1$ from the Active to Firing state.

What is the most important for our model application, we assume that each AP which reaches the AVN propagates further to the rest of the heart: ventricles, causing their contraction. Therefore, the time steps between subsequent AVN excitations are considered as the intervals between the heart beats. These intervals, called further RR-intervals, provide the series the variability of which can be assessed with tools used in quantifying the real signals of heart beats obtained from ECG recordings [35].

4. Simulation results and discussion

Our implementation offers the window-frame, see Fig. 10, in which one can observe the development of the impulse in the SAN, its exit from the SAN and then the impulse propagation over the atrium. The impulse shape is formed by automata in the Firing state which is marked in black. The gray/green color distinguishes automata in the Active state. The white color is used to automata in the Refractory state. The impulse arrival to the AVN is marked by a switch of the color (white to red) of the oval located near the AVN cells. Moreover, one can easy manipulate the values

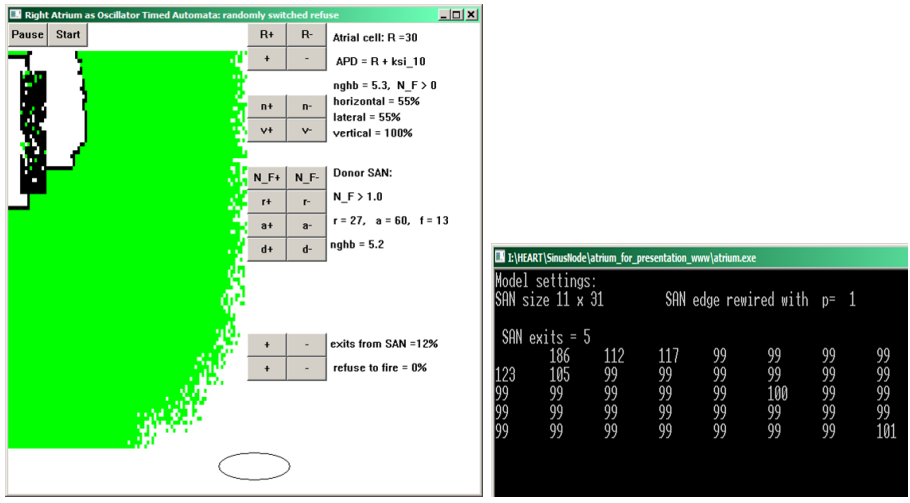

Fig. 10. (Color online) The two windows of our implementation: the interface window and the consola window. The left part of the interface window shows the actual state of the automata with the noticeable rectangle of the SAN cells automata. Gray/green, black and white colors correspond to the Active, Firing and Refractory states of the automata, respectively. Each automaton is represented by 3×5 pixels. The AVN is marked by the oval in the bottom-right. The right part of the interface window provides buttons for model parameter manipulations. The consola window displays the basic model parameters and resulting RR-intervals.

of the crucial model parameters, and observe their impact on the propagation of the impulse. Together the text results of a simulation, identified as RR-intervals, are displayed in the console window.

4.1. Simulation specification

Our simulations were carried out in accordance with the following specification:

— The lattice of size 120×120 was used. The SAN was set to consist of 10×30 cells located at $(10, 10)$, while the AVN was consisted of eight cells located at $(100, 120)$ in a way shown in Fig. 8.

— The system was simulated at different fraction $p_{\text{SAN\_exits}}$ of the SAN to atrium connections. In particular, we started with all connections allowed, and then subsequently considered the exit pathways restricted to 1/2, 1/4, 1/8, 1/16 and 1/32 of all possible. The exit pathways were chosen at random. Notice that at the given size of the SAN, 77 cells could be potentially connected to the atrium.

— The impact of the fraction in possible pathways was observed for different values of cellular refuse to the excitation p_{refuse} and with different densities of atrial non-vertical connections p_{H} and p_{L}. However, in all simulations, the relation $p_{\text{H}} = p_{\text{L}}$ was assumed.

— The intrinsic dynamics of the atrial TA was characterized by the clock constrains: $f = 1$, $r_0 = 30$, $a = 1000$. As ξ was set to 10, the ADP values r_ξ were uniformly distributed in the interval $[30, 40]$.

— The SAN cells rule was driven by: $f^{\text{SAN}} = 13$, $r_0^{\text{SAN}} = 27$, $a^{\text{SAN}} = 60$ and $\xi = 0$. The organization of the SAN intrinsic architecture was the same in all simulations: $p_{\text{V}}^{\text{SAN}} = p_{\text{H}}^{\text{SAN}} = p_{\text{L}}^{\text{SAN}} = 0.65$. Such architecture provided on average 5.2 neighbors for each cell. Moreover, the intercellular connections were modified by *RandomLocalRewiring()* with $p_{\text{rewire}} = 1$, see Fig. 9. The applied rewiring procedure resulted in strong inhomogeneity of the SAN structure. There were always a few cells connected to more than ten other cells, the maximal number of connections was 15 ± 3.

All conditions and values were selected as the best fits to the known physiological observations. Starting with the SAN period $T = f^{\text{SAN}} + r^{\text{SAN}} + a^{\text{SAN}}$ which matched the size of the lattice L, we adjust the fact that under normal conditions, only one wavefront propagates over the right atrium. Then the values of f, r, a were allocated in accordance with the known properties of the myocyte AP.

Thanks to the assumed AVN architecture, *i.e.*, two cells over three cells and over three cells, see Fig. 8, we could specify some extra condition on the impulse which arriving at the AVN is successful in exciting the node. In the following, we considered that the AVN became excited if two of the eight cells of the AVN were simultaneously excited. Notice that, because of the arrangement of the AVN cells, the same impulse could enter the node from the top and from the left side with a few time steps of difference. Obviously, such excitations are not physiologically feasible. To avoid counting fake AVN excitations, we ignored any AVN stimulation which occurred in time shorter than minimal APD, namely shorter than $r_0 = 30$.

4.2. Stationary dynamics and its classification

The variety of observed stationary dynamics was enormous and, in consequence, any automatic classification of these states could potentially be ambiguous. The idea behind the classification below is to stick to the known features of the real heartbeats as close as possible.

The simulations were performed for the large number of different densities of not vertical connections, $p_{\mathrm{nV}} = p_{\mathrm{horizontal}} = p_{\mathrm{lateral}} \in (0.05, 0.95)$, for different levels of cellular impairment $p_{\mathrm{refuse}} \in [0.0, 0.5]$, and at different fraction $p_{\mathrm{SAN\_exit}}$ of SAN to atrium connections. Each parameter setting $(p_{\mathrm{L}} = p_{\mathrm{H}}, p_{\mathrm{refuse}}, p_{\mathrm{SAN\_exits}})$ was simulated a hundred times. Each experiment started from a random initial state of all automata. The first 2000 time steps were left for the system stabilization and then, during the next 2000 steps, the state analysis was performed.

The assumed values for the SAN cell intrinsic activity result that after each $T_{\mathrm{SAN}} = 100$ time steps, the next wave front should leave the SAN. Hence, the perfect score for the AVN excitations should be 20. Accepting the stochastic modifications to the RR-intervals because of r_ξ and local network architecture, and in agreement with the known variability of the RR-intervals in humans [35], we consider any RR-interval with length $80 <$ RR-interval < 120 as **normal** and refer to it as NN.

On the other hand, the finite size of the SAN together with limits in the SAN exit pathways establish circumstances for appearance of the fronts circulating around the SAN. Consequently, there may be observed two wave fronts propagating from the SAN to AVN in place of one wave front. Such a state will be called **SAN-arrhythmia** in connection with the observed SAN tachycardia in humans.

For the classification purposes of any stationary state, in each experiment we count: (a) normal RR-intervals: *count_NN*, (b) RR-intervals shorter than normal: *count_shorter*, (c) RR-intervals longer than normal: *count_longer*, and (d) all observed RR-intervals: *count_RR*. Consequently, RR-

intervals shorter than 80 are assumed as arrhythmic events (tachycardia), RR-intervals longer than 120 are indicates for the arrhythmia with missed beats.

In a series of plots below, we present the screen-shots of typical wave fronts observed in simulations. In each row, we display the same state but at distinct moments of time. The names for the stationary states are based on the characteristics of observed RR-intervals, however they are also consistent with the real heart beat arrhythmia.

— A perfect normal state should satisfy the condition $count\_NN = count\_RR$. However, we accept a deviation from this relation by classifying as normal all states for which $count\_NN > 16$.

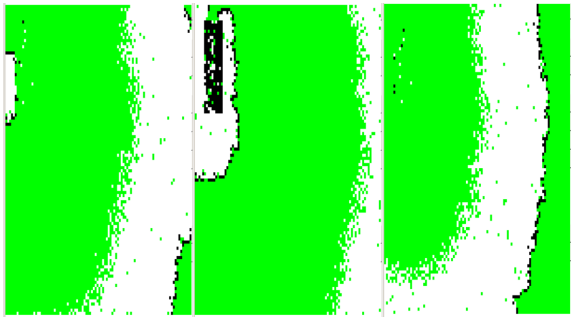

Normal $p_{\mathrm{nV}} = 0.5$, $p_{\mathrm{refuse}} = 0.2$, $p_{\mathrm{SAN\_exits}} = 1/4$. A case of high density of non-vertical connections: one wave front propagates to AVN.

Normal $p_{\mathrm{nV}} = 0.1$, $p_{\mathrm{refuse}} = 0$, $p_{\mathrm{SAN\_exits}} = 1/4$. A case of rare non-vertical connections: few thin fronts slowly propagate to AVN.

— A perfect state of the SAN-arrhythmia should provide $count\_RR = 40$. Again, accepting some distortion from that relation, we classify a state as the SAN-arrhythmia if all RR-intervals are short, *i.e.*, $count\_shorter = count\_RR$.

SAN arrhythmia $p_{\mathrm{nV}} = 0.5$, $p_{\mathrm{refuse}} = 0.2$, $p_{\mathrm{SAN\_exits}} = 1/4$. All RR-intervals are short, two fast fronts propagate to AVN.

— In the case of $count\_RR = count\_shorter + count\_NN$ and $0 < count\_NN \leq 16$, we refer to a state as some other arrhythmia. It can be compared to the supra-ventricular arrhythmia in humans.

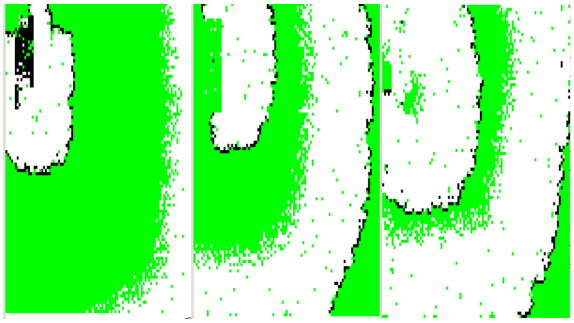

Other arrhythmia $p_{\mathrm{nV}} = 0.5$, $p_{\mathrm{refuse}} = 0.2$, $p_{\mathrm{SAN\_exits}} = 1$. RR-intervals of short and normal length are mixed.

— A state with *count_ shorter* > 0, *count_ longer* > 0 and *count_ RR* > 10 is referred to as arrhythmia with lost beats. At this state, there is often observed, distinct from the SAN, a self-sustained source (multiple sources) of the wave front.

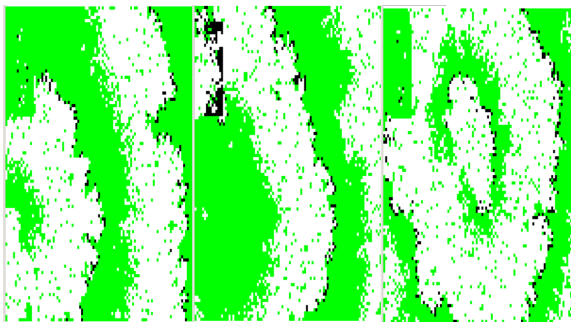

Lost arrhythmia $p_{\mathrm{nV}} = 0.5$, $p_{\mathrm{refuse}} = 0.4$, $p_{\mathrm{SAN\_exits}} = 1$. A case when some other excitation source, different from the SAN, emerges.

— A state with *count_ shorter* > 0, *count_ longer* > 0 and *count_ RR* ≤ 10 is referred to as the lost arrhythmia. Such a state can be compared to the fibrillation phenomenon in the real heart.

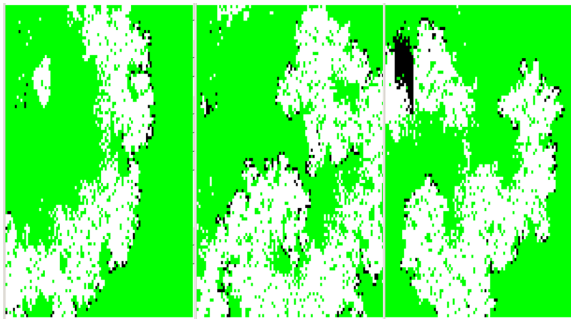

Dead arrhythmia $p_{\mathrm{nV}} = 0.5$, $p_{\mathrm{refuse}} = 0.5$, $p_{\mathrm{SAN\_exits}} = 1$. Many random waves wander but they are inefficient to excite AVN.

— If $6 \leq$ *count_ NN* ≤ 16 and *count_ shorter* $= 0$, the normal rhythm with missed beats is assumed.

— If *count_ NN* < 6 and *count_ shorter* $= 0$, then a state is referred to as the dead normal state.

4.3. Results and discussion

In Fig. 11, we show the probability to observe a final state in the given class. The probabilities are presented for different densities of the network connections $p_{\mathrm{L}} = p_{\mathrm{H}}$, different levels of cellular impairment p_{refuse} and for subsequent ratios of $p_{\mathrm{SAN\_exit}}$.

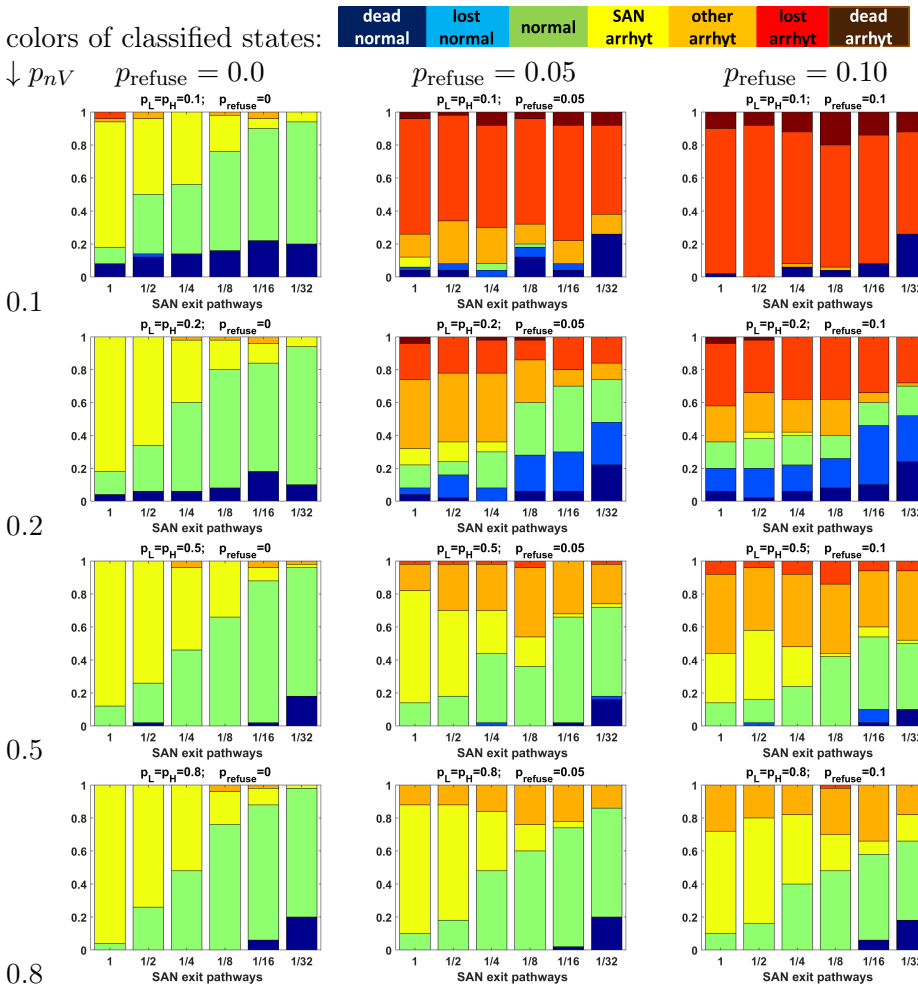

Fig. 11. Table with the distributions of classified states for different density of non-vertical connections, different probability p_{refuse} to refuse stimulation and different ratio of connections between the SAN and atrium $p_{\mathrm{SAN\_exit}}$. In rows of the table the characteristics of systems with the same density p_{nV} (the leftmost numbers give this density) are displayed. In columns, the distributions for systems with the same stochasticity p_{refuse} are plotted.

One can see that all three simulation parameters $p_{\mathrm{L}} = p_{\mathrm{H}}$, p_{refuse}, and $p_{\mathrm{SAN\_exits}}$ influence the state stabilization. In the case of deterministic evolution, when $p_{\mathrm{refuse}} = 0$, the following three limit states dominate: normal, SAN_arrhythmia and dead normal. Their participation seems to be only slightly dependent on the density of non-vertical connections. However, it is noticeable that these distributions strongly depend on $p_{\mathrm{SAN\_exit}}$. It occurs that the fraction of $1/8$ and $1/16$ of SAN exits provides the most stable system, *i.e.*, the probability for the stabilization as a normal state is the greatest.

The described statistics is strongly modified in the case of the stochastic evolution, namely when $p_{\mathrm{refuse}} > 0$. When network connections are rare, $p_{\mathrm{L}} = p_{\mathrm{H}} < 0.2$, the probability for the development of a normal state almost vanishes to 0. Instead, the arrhythmic states: other arrhythmia or lost arrhythmia are found. When the density of network connections seems to be large enough, $p_{\mathrm{L}} = p_{\mathrm{H}} \approx 0.5$, then also the loss in the probability of obtaining stabilization as a normal state is observed. At these densities, the states of other arrhythmia are frequent. The presence of these states only slightly depends on $p_{\mathrm{SAN\_exits}}$ but increases when p_{refuse} increases. Finally, in the case of high density of intercellular connections $p_{\mathrm{L}} = p_{\mathrm{H}} \geq 0.8$, also for stochastic evolution with $p_{\mathrm{refuse}} \leq 0.2$, the system exhibits its ability to stabilize with the normal state at highest probability for $p_{\mathrm{SAN\_exit}} < 1/8$. This property can be read directly from the plots of Fig. 12.

In Fig. 12, we show the probability of the stabilization to the normal rhythm for different parameter settings. From these plots one can see that this probability depends on both the density of non-vertical connections, and probability to refuse an individual cell p_{refuse}. It is noticeable that the level of this probability is strongly related to the fraction of paths from the SAN to atrium $p_{\mathrm{SAN\_exit}}$. In all settings of ($p_{\mathrm{H}} = p_{\mathrm{L}}$, p_{refuse}), the case when all SAN cells were connected to the atrium, $p_{\mathrm{SAN\_exit}} = 1$, led to the negligible number of normal states. For values of $p_{\mathrm{SAN\_exit}} \leq 1/4$, it is not clear from the simulations which value is the optimal one. However, for some specific sets of parameters, it is apparent that the maximum is attained at $p_{\mathrm{SAN\_exit}} = 1/16$, see Fig. 12.

Perhaps, because of the insufficient number of repetitions of simulation experiments and/or the insufficient length of the individual simulation run, the courses of the curves in Fig. 12 are not smooth enough to indicate critical values of the system. Nevertheless, it seems that the isolation of the SAN from atrium provides significantly better conditions for stabilization to the normal rhythm than the complete connection. Additionally, we see that the increasing stochasticity in performance of the cellular rule what mimics cellular impairment, decreases the SAN ability in maintaining the

normal rhythm. Similar results were obtained for the TA system driven by the SAN of different size: smaller (5×15 cells) than the SAN considered here, see [11].

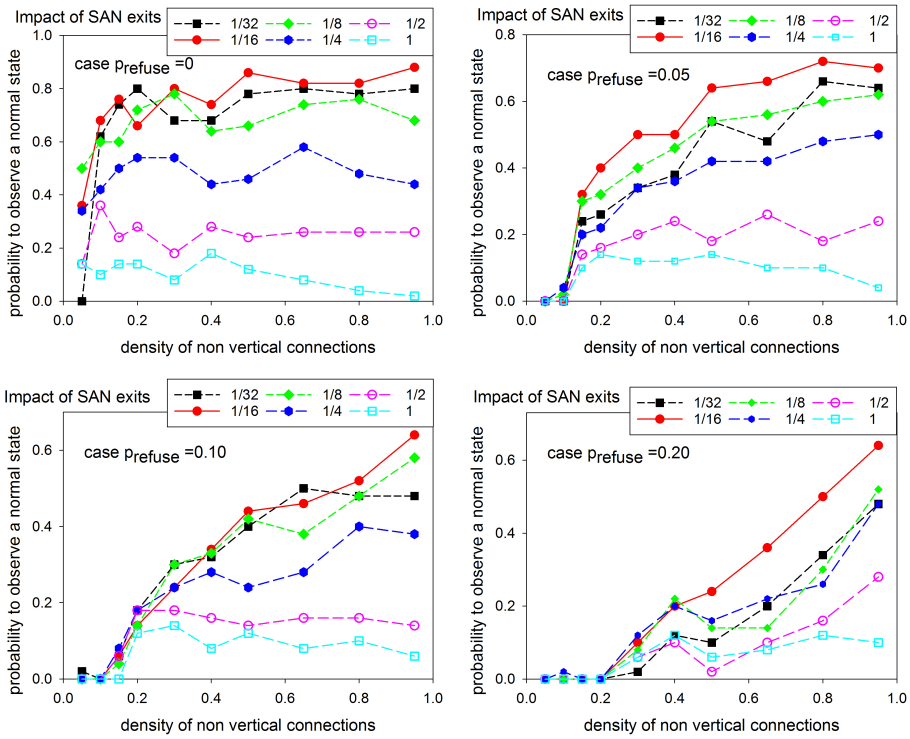

Fig. 12. Probability to observe the stationary state as a normal rhythm for different densities of non-vertical connections. Subsequent panels show this probability for different levels of cellular impairment p_{refuse}.

5. Summary

Although discrete models are often seen as model oversimplification, nevertheless, thanks to their simplicity of design and their comprehensibility, these models allow for a significant advance in our understanding, and provide insights into how to process non-linear, spatially distributed, multiscale dynamical systems. Hybrid automata being a generalization of transition systems are a well-established formalism for modeling and verifying real-time systems acting on both continuous and discrete time scales.

In the case of the AP of a myocyte, the HA approach leads to numerically indistinguishable results from solutions obtained by the continuous methods. However, efficiency of such simulations is ten times better than in the case of the continuous models [30]. Additionally, the HA approach allows to manipulate heterogeneity of both the cellular dynamics and the architecture of intercellular interactions.

Our simulations have provided an important relationship between atrial anatomy and the rhythm of heart excitations. We observed that at a certain probability of possible SAN–atrium pathways (randomly chosen), the occurrence of the normal rhythm attained the highest probability. This property is valid in large intervals for the density of transversal intercellular connections, and for the levels of cellular impairment observed relation. Details of this relation need further extended simulations. After discovering this relation, a backward message can be obtained. Namely, based on the rhythm of heart beats we can conclude about the state of the patient's cardiac tissue.

D.M. gratefully thanks the referee for the constructive comments and recommendations which substantially help improving the readability and quality of the paper.

REFERENCES

[1] R.S. Stephenson *et al.*, *Sci. Rep.* **7**, 7188 (2017).

[2] V.V. Fedorov, A.V. Glukhov, R. Chang, *Am. J. Physiol. Heart Circ. Physiol.* **302**, H1773 (2012).

[3] N. Chandler *et al.*, *Anatom. Rec.* **294**, 970 (2011).

[4] T.A. Csepe *et al.*, *Prog. Biophys. Mol. Biol.* **120**, 164 (2016).

[5] D. Sánchez-Quintana *et al.*, *Heart* **91**, 189 (2005).

[6] S.R. Kharche, E. Vigmond, I.R. Efimov, H. Dobrzynski, *PLOS ONE* **12**, e0183727 (2017).

[7] J. Li *et al.*, *PLOS ONE* **9**, e112547 (2014).

[8] N.A. Trayanova, *Circ. Res.* **114**, 1516 (2014).

[9] D. Makowiec, J. Wdowczyk, Z.R. Struzik, *Front. Physiol.* **9**, 1859 (2019).

[10] D. Makowiec, Atrium: Timed Automata Model of Human Right Atrium Electrophysiology, `https://github.com/DanutaMakowiec/atrium`, 2018.

[11] D. Makowiec, Z.R. Struzik, in: *Computing in Cardiology*, Vol. **45**, P74 2018.

[12] R.E. Klabunde, *Cardiovascular Physiology Concepts*, Lippincott Williams & Wilkins, Wolters Kluwer, 2012.

[13] D. Fatkin, R. Otway, J.I. Vandenberg, *Circulation* **116**, 782 (2007).

[14] C.-H. Luo, Y. Rudy, *Circ. Res.* **74**, 1071 (1994).

[15] T.J. Hund, Y. Rudy, *Circulation* **110**, 3168 (2004).

[16] A.K. Miller *et al.*, *BMC Bioinformatics* **11**, 178 (2010).

[17] G.R. Mirams *et al.*, *J. Physiol.* **594**, 6833 (2016).

[18] Siew Yen Ho, R.H. Anderson, D. Sánchez-Quintana, *Cardiovasc. Res.* **54**, 325 (2002).

[19] Siew Yen Ho, in: *Cardiac Electrophysiology: from Cell to Bedside: Expert Consult — Online and Print*, (Eds.) D.P. Zipes, J. Jalife, Saunders/Elsevier, Philadelphia, PA, US, 2009, Chap. 54, p. 555.

[20] O. Dössel *et al.*, *Med. Biol. Eng. Comput.* **50**, 773 (2012).

[21] Jue Li *et al.*, *Circ. Res.* **102**, 975 (2008).

[22] P. Podziemski, J.J. Żebrowski, *J. Clin. Monit. Comp.* **27**, 481 (2013).

[23] R. FitzHugh, *Biophys. J.* **1**, 445 (1961).

[24] J. Nagumo, S. Arimoto, S. Yoshizawa, *Proceeding IRE* **50**, 2061 (1962).

[25] F. Fenton, A. Karma, *Chaos* **8**, 20 (1998).

[26] J.M. Greenberg, S.P. Hastings, *SIAM J. Appl. Math.* **34**, 515 (1978).

[27] K. Christensen, K.A. Manani, N.S. Peters, *Phys. Rev. Lett.* **114**, 028104 (2015).

[28] K.A. Manani, K. Christensen, N.S. Peters, *Phys. Rev. E* **94**, 042401 (2016).

[29] T.A. Henzinger, in: Proceedings of the 11$^{\text{th}}$ Annual IEEE Symposium on Logic in Computer Science, LICS'96, IEEE Computer Society, Washington, DC, USA, 1996, p. 278.

[30] Pei Ye, E. Entcheva, S.A. Smolka, R. Grosu, *IET Systems Biology* **2**, 24 (2008).

[31] Pei Ye, E. Entcheva, R. Grosu, S.A. Smolka, in: Proceedings of Computational Methods in System Biology, 2005, p. 216.

[32] E. Bartocci, F. Corradini, E. Merelli, L. Tesei, *Theor. Comput. Sci.* **411**, 1999 (2010).

[33] R. Wisniewski, Ch. Sloth, *Model. Ident. Control* **32**, 79 (2011).

[34] D. Makowiec, *Eur. Phys. J. B* **48**, 547 (2005).

[35] TaskForce, *Circulation* **93**, 1043 (1996).